11058 *Inorg. Chem.* **2009**, *48*, 11058–11066
DOI: 10.1021/ic901434u

Inorganic Chemistry
Article

Synthesis of Oxorhenium(V) Complexes with Diamido Amine Ancillary Ligands and Their Role in Oxygen Atom Transfer Catalysis

Yuee Feng, Joel Aponte, Paul J. Houseworth, Paul D. Boyle, and Elon A. Ison*

Department of Chemistry, North Carolina State University, 2620 Yarbrough Drive, Raleigh, North Carolina 27695-8204

Received July 22, 2009

The detailed syntheses of complexes of the form $[Re(O)(X)(RNCH_2CH_2)_2N(Me)]$ (X=Me, Cl, I, R=mesityl, C_6F_5), **1**−**3**, incorporating diamidoamine ancillary ligands are described. X-ray crystal structures for the complexes $[Re(O)(Me)((C_6F_5)NCH_2CH_2)_2N(Me)]$, **1a**, $[Re(O)(I)((C_6F_5)N\ CH_2CH_2)_2N(Me)]$, **3a**, and $[Re(O)(I)((Mes)NCH_2)_2N$-(Me)], **3b**, are reported. The geometry about the metal center in **1a** is best described as a severely distorted square pyramid with the oxo ligand in the apical position. In contrast, the geometry about the metal center in **3a** is best described as a severely distorted trigonal bipyramid, with the iodo ligand occupying the apical position and the diamido nitrogens and the oxo ligand occupying the equatorial plane. The catalytic activities of these complexes for oxygen atom transfer, OAT, from pyridine-*N*-oxides, PyO, to PPh_3 were also examined. The reactions exhibited a clear dependence on the diamido ligand substituent and the X ligand (Me, I, Cl) attached to the metal, with the combined effect that electron-withdrawing substituents on the diamido ligand and poor σ donors directly attached to the metal center increases the rate of catalytic activity. The kinetics of OAT from pyridine-*N*-oxides to Re were also investigated. The reactions displayed clean first order kinetics in Re and saturation kinetics for the dependence on PyO. Changing the PyO substrate had no effect on the saturation value, k_{sat}, suggesting that the OAT reaction in these five-coordinate complexes appears to be governed by isomerization of the starting complex. Attempts to isolate a postulated Re(VII) intermediate were not successful because of hydrolytic degradation. The product of hydrolytic degradation $[((C_6F_5)N(H)CH_2CH_2))_2NH(Me)][X]$, (X=$ReO_4^-$, or I^-), **4** can be isolated, and its X-ray crystal structure is reported. Although the Re(VII) intermediate could not be isolated, its activity in OAT reactions was probed by competition experiments with PPh_3 and four para-substituted triarylphosphines (p-X-Ph)$_3$P (X = OMe, Me, Cl, CF_3). These experiments led to a Hammett that yielded a reaction constant of $\rho = -0.30 \pm 0.01$. This data suggests a positive charge buildup on phosphorus for the OAT reaction and is consistent with the nucleophilic attack of phosphorus on an electrophillic metal oxo.

Introduction

In recent years oxorhenium complexes have been shown to be effective catalysts for oxygen atom transfer, OAT, reactions. Among the complexes that are active for this reaction are $[Re(O)(hoz)_2(CH_3CN)][B(C_6F_5)_4]$ (hoz = 2,(-2′-hydroxyphenyl)-2-oxazoline),[1−5] methyltrioxo rhenium, $MeRe(O)_3$, (MTO),[6−8] and $MeRe(O)$(thiolate)L (L = PAr_3, pyridine, tetramethylthiourea, R_2S).[9−20] These complexes have been

*To whom correspondence should be addressed. E-mail: eaison@ncsu.edu. Phone: (919) 513-4376. Fax: (919) 515-8909.

(1) Corbin, R. A.; Ison, E. A.; Abu-Omar, M. M. *Dalton Trans.* **2009**, *15*, 2850–2855.
(2) Abu-Omar, M. M.; Khan, S. I. *Inorg. Chem.* **1998**, *37*(19), 4979–4985.
(3) Mcpherson, L. D.; Drees, M.; Khan, S. I.; Strassner, T.; Abu-Omar, M. M. *Inorg. Chem.* **2004**, *43*(13), 4036–4050.
(4) Owens, G. S.; Aries, J.; Abu-Omar, M. M. *Catal. Today* **2000**, *55*(4), 317–363.
(5) Abu-Omar, M. M. *Chem. Commun.* **2003**, *17*, 2102–2111.
(6) Herrmann, W. A.; Rost, A. M. J.; Mitterpleininger, J. K. M.; Szesni, N.; Sturm, S.; Fischer, R. W.; Kuhn, F. E. *Angew. Chem., Int. Ed.* **2007**, *46* (38), 7301–7303.
(7) Rost, A. M. J.; Herrmann, W. A.; Kuehn, F. E. *Tetrahedron Lett.* **2007**, *48*(10), 1775–1779.
(8) Abu-Omar, M. M.; Appelman, E. H.; Espenson, J. H. *Inorg. Chem.* **1996**, *35*(26), 7751–7757.
(9) Wang, Y.; Espenson, J. H. *Org. Lett.* **2000**, *2*(22), 3525–3526.
(10) Espenson, J. H.; Nabavizadeh, S. M. *Eur. J. Inorg. Chem.* **2003**, *10*, 1911–1916.
(11) Dixon, J.; Espenson, J. H. *Inorg. Chem.* **2002**, *41*(18), 4727–4731.
(12) Lente, G.; Espenson, J. H. *Inorg. Chem.* **2000**, *39*(21), 4809–4814.
(13) Wang, Y.; Espenson, J. H. *Inorg. Chem.* **2002**, *41*(8), 2266–2274.
(14) Shan, X. P.; Ellern, A.; Guzei, I. A.; Espenson, J. H. *Inorg. Chem.* **2004**, *43*(13), 3854–3862.
(15) Cai, Y.; Ellern, A.; Espenson, J. H. *Inorg. Chem.* **2005**, *44*(7), 2560–2565.
(16) Vasbinder, M. J.; Espenson, J. H. *Organometallics* **2004**, *23*(13), 3355–3358.
(17) Abu-Omar, M. M.; Espenson, J. H. *J. Am. Chem. Soc.* **1995**, *117*(1), 272–280.
(18) Espenson, J. H. *Adv. Inorg. Chem.* **2003**, *54*, 158−202.
(19) Espenson, J. H. *Coord. Chem. Rev.* **2005**, *249*(3−4), 329–341.
(20) Shan, X. P.; Ellern, A.; Guzei, I. A.; Espenson, J. H. *Inorg. Chem.* **2003**, *42*(7), 2362–2367.

Published on Web 11/04/2009

Chart 1

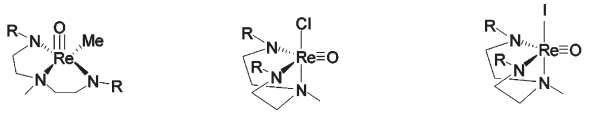

R = C_6F_5, **1a**; R = Mes, **1b** R = C_6F_5, **2a**; R = Mes, **2b** R = C_6F_5, **3a**; R = Mes, **3b**

utilized in a wide variety of reactions, including epoxidations,[21,22] aldehyde olefinations,[23−26] oxidations of sulfur containing species,[2,27,28] and even the reduction of perchlorates.[3,29] The utility of rhenium complexes for these reactions lies in the fact that unlike catalysts that incorporate the isoelectronic group 6 metals (Mo, and W),[30] that are prevalent in biological oxotransferases, the kinetics of OAT with rhenium is facile and occurs at non-forcing conditions.

The known OAT rhenium catalysts incorporate terminal oxo and ancillary ligands such as thiolates, and oxazolines. While these complexes are effective, a major limitation is that the ancillary ligands do not allow for tuning the sterics and electronics around the metal center so that systematic improvements to the catalytic activity can be made. To address this issue, we have synthesized a series of oxorhenium complexes of the form $[Re(O)(X)(RNCH_2CH_2)_2N(Me)]$ (X = Me, Cl, I; R = mesityl, C_6F_5; Chart 1), that incorporate diamidoamine ancillary ligands.

The design of these complexes allows for a systematic investigation of the catalytic activity as the electronics and sterics of the X substituent on the metal and the R substituent on the diamido ligand are varied. In this article we examine the kinetics of OAT for six oxorhenium complexes incorporating diamidoamine ancillary ligands. We describe in detail the syntheses of these complexes, examine the structural consequences of varying the electronics at the metal center, investigate in detail the mechanism for OAT from pyridine-*N*-oxides, and compare the catalytic activities of these complexes for OAT from pyridine-*N*-oxides to PPh_3.

Results and Discussion

Syntheses of Complexes. Diamidoamines have been utilized as ligands for early transition metal olefin polymerization and metathesis catalysts.[31−35] We were attracted to them because of the ease of synthesis, and the fact that the electronics and sterics at the amido nitrogens could be easily varied. Oxorhenium complexes incorporating these ligands were synthesized according to the methods outlined in Scheme 1.

Methyl rhenium complexes **1a**−**b** were prepared by treating a dichloromethane solution of $MeRe(O)_3$, MTO, with 1 equiv of PPh_3 and an equivalent of the appropriate ligand, and allowing the solution to stand at room temperature overnight. This procedure, led to black crystals of **1**, which in the case of **1a** were suitable for single-crystal X-ray diffraction studies. Complex **1** is stable in air.

The chlororhenium complex $Re(O)Cl(MesNCH_2CH_2)_2NMe$ (**2b**) was obtained as a yellow solid from mer-$Re(O)Cl_3(PPh_3)_2$, $MeN((MesN(H)(CH_2)_2)_2$, and 2 equiv of 2,6-lutidine, in refluxing ethanol for 16 h. The synthesis of complex **2a** was previously reported by Schrock and co-workers from the reaction of $[Re(O)Cl_4][NBu_4]$ and the ligand $MeN(C_6F_5NH(CH_2)_2)_2$.[33] We have found, however, that **2a**, an air-stable green solid, can be more conveniently prepared by stirring a suspension of mer-$Re(O)Cl_3(PPh_3)_2$ and $MeN(C_6F_5N(H)(CH_2)_2)_2$ at room temperature for 5 days.

Finally the green iodorhenium complexes **3** were obtained by stirring a suspension of purple $Re(O)_2I(PPh_3)_2$, and 1 equiv of the appropriate ligand, in dichloromethane for 12 h. These air-stable complexes were isolated as powders after filtration to remove any unreacted starting material, concentration of the filtrate, and precipitation with hexanes. All complexes were fully characterized by ^1H, ^{13}C or ^{19}F NMR and elemental analysis. Complexes **1a**, **3a**, and **3b** were also characterized by X-ray crystallography.

Crystallographic Studies. As mentioned above, crystals of **1a** suitable for X-ray crystallography were obtained by allowing the reaction mixture to stand at room temperature for 12 h. Crystals of **3a** and **3b** were obtained by slow diffusion of pentane into a concentrated CH_2Cl_2 solution at room temperature. The crystal structure of **2a** was previously reported.[33] Interesting structural differences are apparent when complex **1a** is compared to the halide containing complexes **2a**, **3a**, and **3b**.

The geometry about the metal center in **1a** is best described as a severely distorted square pyramid with the oxo ligand in the apical position (Figure 1). The Re−O bond length (1.685(4) Å) is consistent with the assignment of a triple bond.[36−39] The Re atom lies 0.7184(2) Å above the plane made by the atoms N1, N2, N2a, and C1.

In contrast, the geometry about the metal center in **3a** is best described as a severely distorted trigonal bipyramid (Figure 2), with the iodo ligand occupying the apical position and the atoms, N2, N3 and O1, occupying the equatorial plane. The angles for the atoms in the equatorial

(21) Zhou, M. D.; Zhao, J.; Li, J.; Yue, S.; Bao, C. N.; Mink, J.; Zang, S. L.; Kuehn, F. E. *Chem.—Eur. J.* **2007**, *13*(1), 158–166.
(22) Gisdakis, P.; Antonczak, S.; Kostlmeier, S.; Herrmann, W. A.; Rosch, N. *Angew. Chem., Int. Ed.* **1998**, *37*(16), 2211–2214.
(23) Kuhn, F. E.; Santos, A. M. *Mini-Rev. Org. Chem.* **2004**, *1*(1), 55–64.
(24) Pedro, F. M.; Hirner, S.; Kuhn, F. E. *Tetrahedron Lett.* **2005**, *46*(45), 7777–7779.
(25) Santos, A. M.; Romao, C. C.; Kuhn, F. E. *J. Am. Chem. Soc.* **2003**, *125*(9), 2414–2415.
(26) Santos, A. M.; Pedro, F. M.; Yogalekar, A. A.; Lucas, I. S.; Romao, C. C.; Kuhn, F. E. *Chem.—Eur. J.* **2004**, *10*(24), 6313–6321.
(27) Schultz, B. E.; Hille, R.; Holm, R. H. *J. Am. Chem. Soc.* **1995**, *117*(2), 827–828.
(28) Arterburn, J. B.; Perry, M. C.; Nelson, S. L.; Dible, B. R.; Holguin, M. S. *J. Am. Chem. Soc.* **1997**, *119*(39), 9309–9310.
(29) Abu-Omar, M. M.; Mcpherson, L. D.; Arias, J.; Bereau, V. M. *Angew. Chem., Int. Ed.* **2000**, *39*(23), 4310.
(30) Enemark, J. H.; Cooney, J. J. A. *Chem. Rev.* **2004**, *104*(2), 1175–1200.
(31) Cochran, F. V.; Schrock, R. R. *Organometallics* **2001**, *20*(11), 2127–2129.
(32) Cochran, F. V.; Hock, A. S.; Schrock, R. R. *Organometallics* **2004**, *23*(4), 665–678.
(33) Cochran, F. V.; Bonitatebus, P. J.; Schrock, R. R. *Organometallics* **2000**, *19*(13), 2414–2416.
(34) Lopez, L. P. H.; Schrock, R. R.; Bonitatebus, P. J. *Inorg. Chim. Acta* **2006**, *359*(15), 4730–4740.
(35) Guerin, F.; Mcconville, D. H.; Vittal, J. J.; Yap, G. A. P. *Organometallics* **1998**, *17*(23), 5172–5177.
(36) Herrmann, W. A.; Roesky, P. W.; Wang, M.; Scherer, W. *Organometallics* **1994**, *13*(11), 4531–4535.
(37) Herrmann, W. A.; Ding, H.; Kuhn, F. E.; Scherer, W. *Organometallics* **1998**, *17*(13), 2751–2757.
(38) Herrmann, W. A.; Correia, J. D. G.; Rauch, M. U.; Artus, G. R. J.; Kuhn, F. E. *J. Mol. Catal. A: Chem.* **1997**, *118*(1), 33–45.
(39) Romao, C. C.; Kuhn, F. E.; Herrmann, W. A. *Chem. Rev.* **1997**, *97*(8), 3197–3246.

Scheme 1

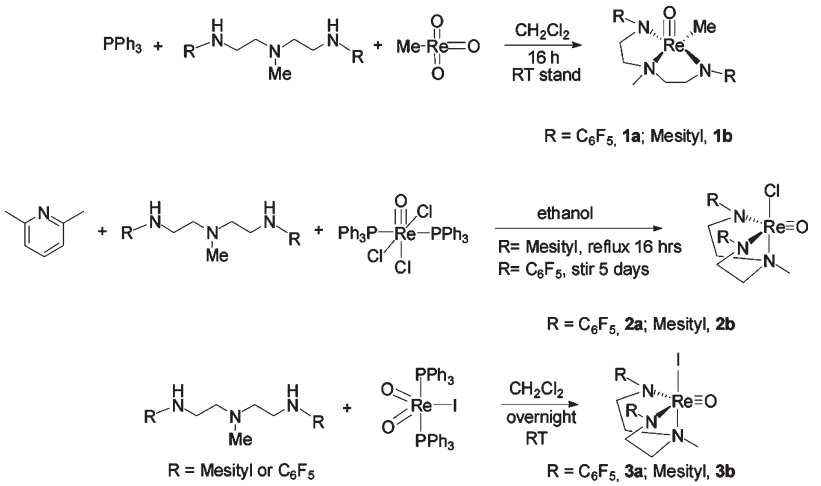

plane, O1−Re1−N2, 120.04(12); O1−Re1−N3, 119.63(12); N2−Re1−N3, 118.44(11), are all consistent with a trigonal bipyramidal geometry. In comparison, for complex **1a**, these angles are O1−Re1−N2, 113.08(9); O1−Re1−N2a, 113.08(9); N2−Re1−N2a, 133.43(17). The I1−Re1−N1 angle in **3a** is 163.23(7)° which is distorted by 17° from the idealized angle in a trigonal bipyramid. However, for complex **1a** this distortion is significantly more severe (C1−Re1−N1, 143.36(18)). The crystal structure for **3b** (Supporting Information), which contains mesityl substituents on the diamido ligand is very similar to **3a**, and the geometry about the metal center can again be described as a severely distorted trigonal bipyramid. Thus the preference for a square pyramidal geometry versus a trigonal bipyramidal geometry seems to arise from the electronics of the X ligand directly attached to the metal center and not from the diamido substituents. The preference for a trigonal bipyramidal geometry in **3a** and **3b** is due to the increased stability in a trigonal bipyramidal crystal field that occurs when an electronegative atom (Cl, I) is placed in the apical position. The methyl complex, **1a**, encounters a larger crystal field splitting when the high-field ligand, methyl, is in the basal plane of a square pyramid as opposed to in the apical position in the TBP structure.[40]

Catalytic OAT. To investigate the effect of substituents on catalytic activity in OAT reactions we examined the reactivity of catalyst **1**−**3** for the catalytic OAT from pyridine-*N*-oxides to PPh_3 according to eq 1.

$$PPh_3 + PyO \xrightarrow{\text{catalyst}} OPPh_3 + Py \qquad (1)$$

Reactions were performed at room temperature in CD_2Cl_2 (1 mL) with 1 mol % catalysts (0.0054 mmol), PPh_3 (0.54 mmol), and PyO (0.65 mmol). The disappearance of PPh_3 and the appearance of $OPPh_3$ was monitored by ^{31}P NMR. As shown in Figure 3, there is a clear dependence in OAT reactions on substituents on the diamido ligand and the X ligand (Me, I, Cl) attached to the metal center. This dramatic effect is seen when complexes **3a**, [Re(O)(I)((C$_6$F$_5$)NCH$_2$CH$_2$)$_2$N(Me)], are compared with **1b**, [Re(O)(Me)((Mes)NCH$_2$CH$_2$)$_2$N(Me)]. With 1 mol % catalyst, PPh_3 is completely converted to $OPPh_3$ by **3a** in less than 10 min. In contrast, less than 10% of PPh_3 is converted to $OPPh_3$ after 6 h by **1b** under the same reaction conditions. Thus the combined effect of electron withdrawing substituents on the diamido ligand and poor σ donors directly attached to the metal center appears to dramatically increase the rate of catalytic activity. This is exemplified further when complex **3a**, [Re(O)(I)((C$_6$F$_5$)NCH$_2$CH$_2$)$_2$N(Me)], is compared with **3b**, [Re(O)(I)((Mes)NCH$_2$CH$_2$)$_2$N(Me)] and complex **1a**, [Re(O)(Me)((C$_6$F$_5$)NCH$_2$CH$_2$)$_2$N(Me)] is compared with **1b**, [Re(O)(Me)((Mes)NCH$_2$CH$_2$)$_2$N(Me)]. Complex **3a** converts 100% of PPh_3 to $OPPh_3$ in 10 min while this conversion is achieved with **3b** in 250 min. Similarly, 10% of PPh_3 is converted to $OPPh_3$ within 2 min by **1a**, while complex **1b** requires 350 min to convert the same amount of PPh_3. Thus the general trend from the catalytic data is **3a** ≈ **2a** > **1a** > **3b** > **2b** > **1b**. From the data, changing the substituent on the diamido ligand appears to have a more dramatic effect on the rate of catalysis.

A drawback of this catalytic system especially for the halide complexes, **2**−**3**, is that the complexes are susceptible to hydrolytic degradation. This is seen in Figure 3 when the halo complexes **2a** and **3a** are compared. While both complexes appear initially to perform at approximately the same rate, after 10 min **3a** reaches its maximum conversion (≈75%). In fact, the maximum conversion for both **3a** and **2a** varies depending on the amount of water present in the solvent. An ESI-MS of the reaction mixture after a catalytic run revealed the presence of ReO_4^-, and protonated ligand, ((C$_6$F$_5$)N(H)CH$_2$CH$_2$)$_2$NH(Me)).

Mechanism of OAT. The generally accepted mechanism for transition metal catalyzed OAT usually involves the formation of a high-valent transition metal oxo intermediate which subsequently reacts with an oxygen atom acceptor.[3,11−13,19,41] As depicted in Figure 4 the catalytic cycle can be divided into two halves; one-half involves oxidation of the metal center by an oxygen atom donor, while the other half involves oxidation of the substrate by a high-valent metal oxo intermediate.

(40) Albright, T. A.; Burdett, J. K.; Whangbo, M.-H. *Orbital Interactions in Chemistry*; John Wiley and Sons: New York, 1999.

(41) Arias, J.; Newlands, C. R.; Abu-Omar, M. M. *Inorg. Chem.* **2001**, *40* (9), 2185–2192.

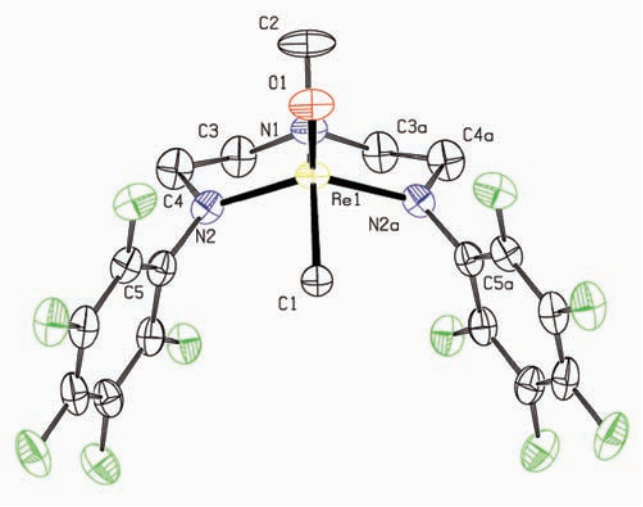

Figure 1. X-ray single crystal structure of Re(O)(Me)((C$_6$F$_5$)NCH$_2$-CH$_2$)$_2$N(Me)], **1a**. Thermal ellipsoids are 50%. Selected bond distances (Å) and angles (deg). Re1−O1, 1.685(4); Re−N2, 1.972(3); Re−C1, 2.122(5); Re−N1, 2.162(4); O1−Re1−N2, 113.08(9); N2−Re1−N2a, 133.43(17); O1−Re1−N1, 112.43(17); N2−Re1−N1, 78.70(9), C1−Re1−N1, 143.36(18); O1−Re1−C1, 104.20(18).

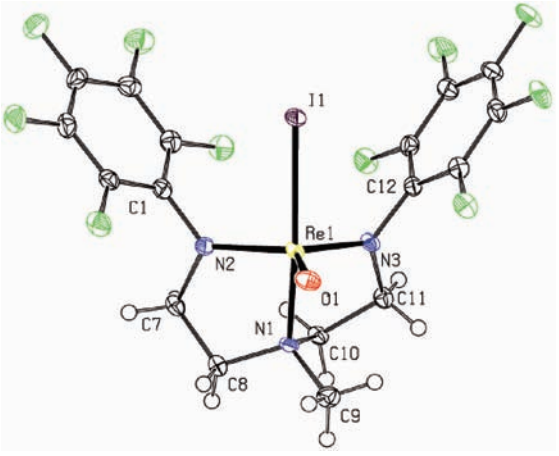

Figure 2. X-ray single crystal structure of Re(O)(I)((C$_6$F$_5$)-NCH$_2$CH$_2$)$_2$N(Me)], **3a**. Thermal ellipsoids are 50%. Selected bond distances (Å) and angles (deg). Re1−O1, 1.691(2); Re1−N2, 1.950(3); Re1−I1, 2.6954(3); Re1−N1, 2.127(3); O1−Re1−N2, 120.04(12); O1−Re1−N3, 119.63(12); N2−Re1−N3, 118.44(11); N2−Re1−N1, 79.39(11); N3−Re1−N1, 79.84(11); O1−Re1−I1, 99.66(8); N1−Re1−I1, 163.23(7).

The observation that the catalytic reaction is more facile for catalysts with electron-withdrawing substituents on the diamido ligand, and poor σ donor X ligands suggests that for this system the substrate oxidation/metal reduction step is turnover limiting.

To investigate the kinetics of OAT in these complexes and to examine the effects that substituents have on both halves of the catalytic cycle, we investigated in detail the mechanism for both the OAT from pyridine-*N*-oxide and its derivatives, and the OAT from the putative Re(VII) intermediate to PPh_3.

OAT from Pyridine-*N*-oxides to Re(V). The reactions of **2a** (Scheme 2) with pyridine-*N*-oxide were investigated under pseudo-first-order conditions using UV−vis spectroscopy.

The progress of the reaction was monitored at 368 nm, where the rhenium(V) oxo-chloro complex, **2a**, absorbs

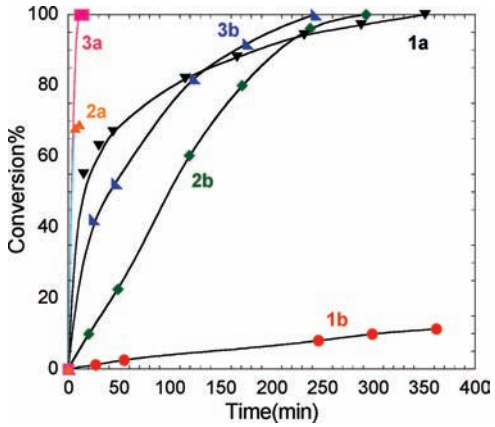

Figure 3. Catalytic OAT with catalysts **1**−**3** for the reaction of PPh_3 with PyO according to the equation 1. Reactions were performed with 1 mol % catalyst (0.0054 mmol) based on PPh_3 (0.54 mmol) and 1.2 equiv. of PyO (0.65 mmol) in CD_2Cl_2 (1 mL) at room temperature. Reactants and products were monitored by ^{31}P NMR spectroscopy. Conversion % refers to the relative ratio of $OPPh_3$:PPh_3.

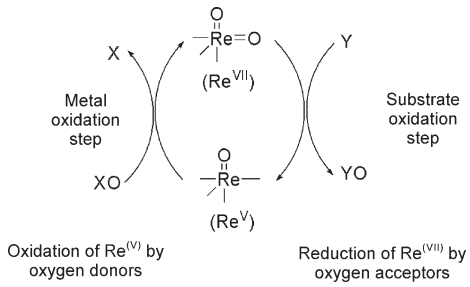

Figure 4. Simplified mechanism for OAT with oxorhenium complexes.

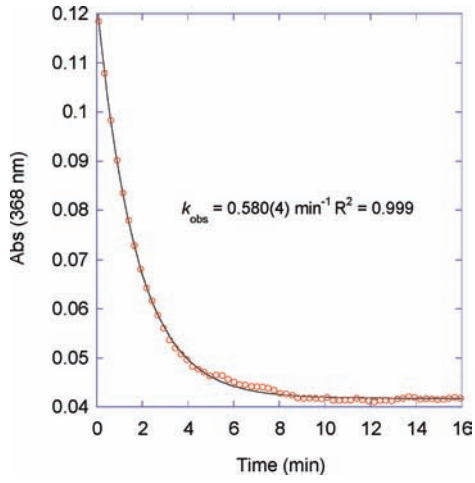

Figure 5. Typical absorbance versus time plot for the reaction of **2a** with PyO. Reactions were performed at 298 K in CH_3CN at 368 nm. Conditions were [Re] = 0.3 mM, [PyO] = 0.05 M. The k_{obs} values were obtained by non-linear fitting of Abs_{368} versus time to the equation: $Abs_t = Abs_\infty + (Abs_0 - Abs_\infty)\exp(-k_{obs}t)$.

Scheme 2

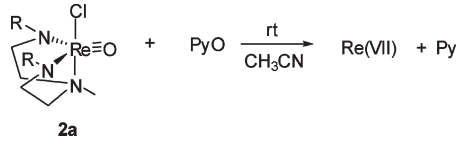

2a

but the product does not (see Supporting Information). The disappearance of **2a** monitored at 368 nm displayed clean first order kinetics in Re (Figure 5). A plot of k_{obs} versus [PyO] revealed saturation kinetics for the dependence on PyO (Figure 6).

Saturation kinetics in PyO is consistent with several kinetically indistinguishable mechanisms that are depicted in Scheme 3. From the crystal structure for **2a** and **3a** the metal-halide bonds are particularly long. This suggests that these bonds may be weak and thus a plausible mechanism (Scheme 3A) could involve dissociation of the halide ligand to produce a cationic 14 electron intermediate which quickly reacts with PyO to produce the Re(VII) dioxo species.

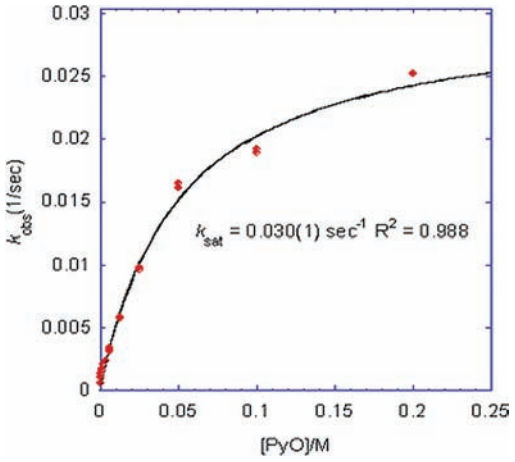

Figure 6. PyO dependence for the reaction of PyO with **2a** in CH_3CN at 298 K. Conditions were [Re] = 0.3 mM, [PyO] = 0.015 M−0.2 M. Data was fit with non-linear least-squares fitting to an equation describing saturation in [PyO]: $k_{obs} = k'[PyO]/(k'' + [PyO])$.

Two alternative mechanisms (Scheme 3B and Scheme 3C) involve isomerization of the starting complex prior to oxidation by PyO. In the mechanism depicted in Scheme 3B, the amine ligand dissociates from the metal in a prior equilibrium step to form a 14-electron intermediate, which subsequently reacts with PyO to form the products. In Scheme 3C, the complex rearranges to create an open coordination site cis to the Re−O bond. As described earlier, the solid state structures described for **1a**, **2a**, **3a**, and **3b** are characterized by different isomers depending on the ligands attached to the metal. Thus, geometrical isomerization prior to OAT to Re by PyO is a reasonable hypothesis.

The last mechanism in Scheme 3 (Scheme 3D) is associative, involving attack of the PyO ligand cis to Re−O bond to form, in a prior equilibrium step, an adduct of PyO where this ligand is cis to the oxo and the Cl ligand is trans. This is then followed by OAT to form Re(VII).

To investigate these mechanisms further, we compared the kinetic behavior of five different *para*-substituted pyridine-*N*-oxides, 4-X-PyO, (X = Me, H, phenyl, CN, OMe). Changing the PyO substrate would have an effect on the saturation value, k_{sat}, in Scheme 3D, as the saturation value is governed by k_8. However, changing the substrate would not affect the saturation values k_1, k_3, and k_5 according to Schemes 3A−C. As shown in Table 1 changing the para substituent on the PyO does not affect the saturation value. Thus the data precludes mechanism Scheme 3D.

In addition, the temperature dependence of the rate constant k_{sat} was also investigated from 288 to 308 K. From this analysis the entropy of activation, $\Delta S^{\ddagger}$, was

Scheme 3

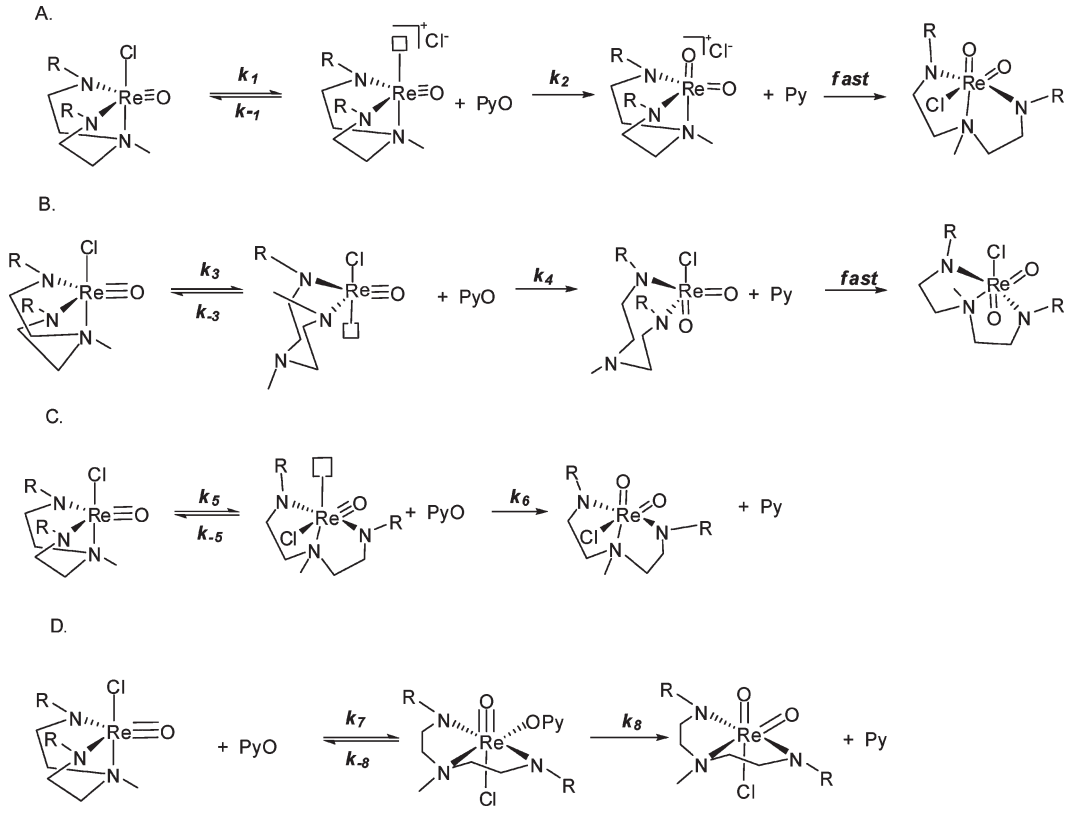

Table 1. Comparison of Saturation Rate Constants for the Reaction of **2a** with para-Substituted Pyridine-*N*-oxides for the Reaction

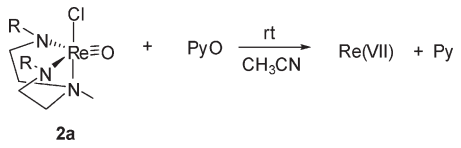

2a

substrate	$^{a}k_{sat}$ (s^{-1})
PyO	0.030(1)
CN-PyO	0.030(1)
Ph-PyO	0.021(2)
Me-PyO	0.039(8)
OMe-PyO	0.034(6)

[a] Saturation rate constants obtained by non-linear fits to the equation: rate $= -d[Re]/dt = \{k_{sat}[Re][PyO]\}/\{K' + \{pyO]\}$.

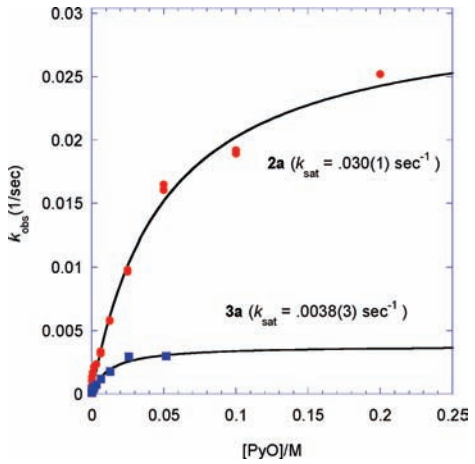

Figure 7. Comparison of saturation rate constants, k_{sat}, between **2a** and **3a**.

found to be negative (−16.7 eu) while the enthalpy of activation, $\Delta H^{\ddagger}$ was positive (14.4 kcal/mol.K). These activation parameters are not consistent with the dissociative pathway depicted in Scheme 3A.[42] Further, as shown in Figure 7, the rate constant at saturation (k_{sat}) for **2a** is about 8 times larger than for **3a**, this is again not consistent with Scheme 3A as one would expect I^-, the better leaving group, to dissociate more readily than Cl^- if dissociation of the halide ligand were the operational mechanism.

Thus the mechanisms depicted in Schemes 3B and Scheme 3C are the only viable mechanisms. While we prefer mechanism C, primarily because it avoids a high energy 14-electron intermediate, this mechanism cannot be ruled out with the available data. In any event, the saturation kinetics of the PyO substrate in the OAT reaction in these five-coordinate complexes appears to be governed by isomerization of the starting complex. This is, in contrast to the six-coordinate complexes $[Re(O)(hoz)_2(CH_3CN)][B(C_6F_5)_4]$, reported by Abu-Omar and co-workers, where saturation is governed by the oxidation from Re(V) to Re(VII).[3] A rate equation

Scheme 4

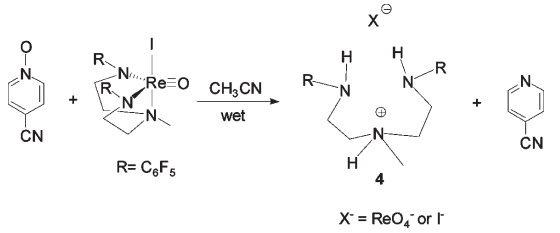

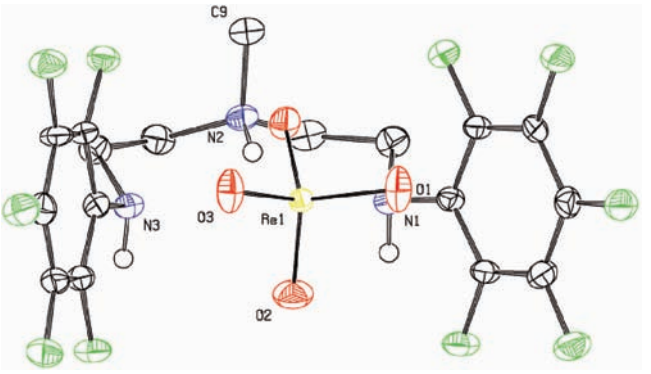

Figure 8. X-ray single crystal structure $[(C_6F_5)(NHCH_2CH_2)_2HN(Me)][ReO_4]$, **4**. Thermal ellipsoids are 50%. The structure exhibits a compositional disorder in ReO_4^- and I^-. The I^- ion is not shown.

based on mechanism C that is consistent with the experimental data is depicted in eq 2, where $k_{sat} = k_5$ and $K' = k_{-5}/k_6$.

$$\text{rate} = \frac{-d[Re]}{dt} = \frac{k_{sat}[Re][PyO]}{K' + [PyO]} \qquad (2)$$

$$k_{sat} = k_5$$

$$K' = k_{-5}/k_6$$

OAT from Re(VII) to PPh_3. As mentioned above the traditional mechanism for OAT involves initial oxidation of the metal to Re(VII) by an oxygen atom donor, followed by the transfer of an oxo from this high-valent Re intermediate to an oxygen atom acceptor.[3,11−13,19,27,41,43] Despite several attempts the postulated Re(VII) intermediate could not be isolated in these complexes as the hydrolytic degradation of this intermediate quickly ensued. As an illustration, when **3a** is treated with 4-cyanopyridine-*N*-oxide, a color change from green to red quickly takes place. However, isolation of the red product and crystallization by slow diffusion of Et_2O into a concentrated acetonitrile solution of this complex at room temperature results in the formation of $[(C_6F_5)(N(H)CH_2CH_2)_2NH(Me)][X]$, ($X = ReO_4^-$, or I^-), **4** (Scheme 4).

The X-ray structure (Figure 8) confirms the assignment of **4**, although the structure exhibits a compositional disorder in ReO_4^- and I^-. ^1H and ^{19}F NMR data along with elemental analysis are also consistent with the assignment for this molecule. Similarly, the treatment of complex **2a** and **3b** with pyridine-*N*-oxide results in an initial color change from green to red, and then over

(42) *Inorganic and Organometallic Reaction Mechanisms*; Atwood, J. D, Ed.; VCH: New York, 1997; p 13.

(43) Abu-Omar, M. M. *Comments Inorg. Chem.* **2003**, *24*(1), 15–37.

Scheme 5

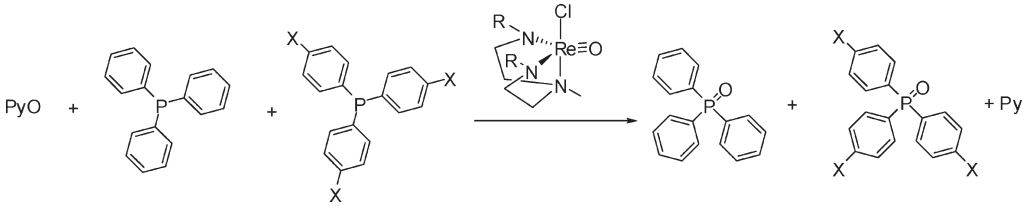

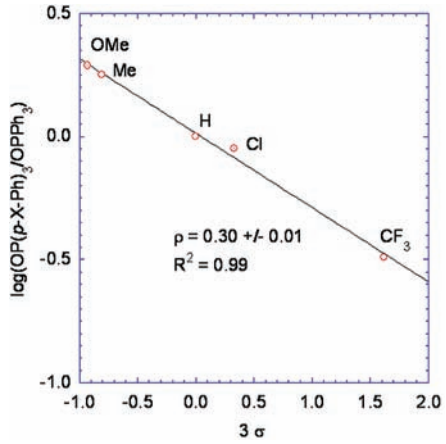

Figure 9. Hammett Plot obtained from competition experiments with para-substituted triaryl phosphines (p-X-Ph)$_3$P (X = OMe, Me, Cl, CF_3) as depicted in Scheme 4. The ratio of products was obtained by integration of the ^{31}P NMR spectrum for each experiment.

longer periods of time to yellow. The ^{1}H NMR spectrum of these solutions reveals the presence of free ligand.

Although the Re(VII) intermediate could not be isolated, its activity in OAT reactions was probed by competition experiments with PPh_3 and four para-substituted triarylphosphines (p-X-Ph)$_3$P (X = OMe, Me, Cl, CF_3) as depicted in Scheme 5. Reactions were performed in CD_3CN at room temperature with the ratio of Re/PyO/PPh_3:(p-X-Ph)$_3$P = 1:20:100:100. The ratio of $OPPh_3$/(p-X-Ph)$_3$PO was determined by integration of the ^{31}P NMR spectrum for each experiment. From the relative ratios of the products a Hammett plot (Figure 9) that yielded a reaction constant of -0.30 ± 0.01 was obtained. This data suggests a positive charge buildup on phosphorus for the OAT reaction and is consistent with the nucleophilic attack of phosphorus on an electrophillic metal oxo.[13,44,45]

Conclusion

We have demonstrated that oxorhenium complexes of the form [Re(O)(X)(RNCH$_2$CH$_2$)$_2$N(Me)] (X = Me, Cl, I, R = mesityl, C_6F_5), incorporating diamidoamine ancillary ligands, can be effectively tuned for OAT reactions by varying the electronics of the amido substituents and the nature of the X ligand attached directly to the metal. Catalytic OAT is favored by electron-withdrawing substituents on the amido nitrogens and poor σ donors attached directly to the metal. The rate of OAT in these complexes is governed by isomerization of the metal complex rather than oxidation of the metal as observed by Abu-Omar and co-workers.[3] The data presented suggests that the catalytic OAT reactions presented proceed via the generation of an electrophillic high-valent Re oxo species. The catalytic efficiency of these complexes is thwarted, however, by the high reactivity of this species and its susceptibility to hydrolytic degradation.

Experimental Section

Reagents and Instrumentation. Ligands (MesNHCH$_2$CH$_2$)$_2$NMe[46] and (C_6F_5NHCH$_2$CH$_2$)$_2$NMe[33] and complexes Re(O)Cl(C_6F_5NCH$_2$CH$_2$)$_2$NMe[33] and Re(O)$_2$I(PPh$_3$)$_2$[47] were prepared as previously reported. Other reagents were purchased from commercial sources and used as received. Solvents were degassed and purified with a solvent purification system (MBraun Inc.) prior to use. ^{1}H and ^{13}C, ^{31}P and ^{19}F NMR spectra were recorded on a Varian Mercury 400 MHz or a Varian Mercury 300 MHz spectrometer. All ^{1}H and ^{13}C NMR spectra were referenced against tetramethylsilane using resonances due to the residual protons in the deuterated solvents or the ^{13}C resonances of the deuterated solvents. ^{31}P NMR spectra were obtained on a Varian spectrometer operating at 162 MHz and referenced against external 85% H_3PO_4. ^{19}F NMR spectra were obtained on a Varian spectrometer operating at 377 MHz and referenced against the external standard C_6F_6 (163 ppm). Unless otherwise noted, NMR spectra were acquired at room temperature. Elemental analyses were performed by Atlantic Microlabs, Inc. UV−vis spectra were recorded on a Cary 100 Bio spectrophotometer equipped with a thermostatted 6 × 6 multicell peltier. Mass spectrometry was performed by the NC State Mass Spectrometry Facility. X-ray crystallography was performed at the X-ray Structural Facility of North Carolina State University. Data fitting was done using KaleidaGraph 4.0 software.

Re(O)Me(C_6F_5NCH$_2$CH$_2$)$_2$NMe (1a). Triphenylphosphine (262.3 mg, 0.802 mmol), (C_6F_5NHCH$_2$CH$_2$)$_2$NMe (326.7 mg, 0.802 mmol), and methyltrioxorhenium (200 mg, 0.802 mmol) were added sequentially to a small reaction vial with about 2 mL of dichloromethane. The product was allowed to crystallize for 16 h to yield purple crystals (138 mg, 27.6%). ^{1}H NMR (acetone-d_6, δ): 4.47 (m, 2H, NCH_2CH$_2$N), 3.77(m, 2H, NCH_2CH$_2$N), 3.51(s, 3H, N−CH_3), 3.32 (m, 2H, NCH_2CH$_2$N), 2.83 (m, 2H, NCH_2CH$_2$N), 2.21 (s, 3H, Re−CH_3). ^{19}F NMR (acetone-d_6, δ): −151.15 (m, 4F, phenyl-F), −164.573 (m, 2F, phenyl-para-F), −167.07 (m, 4F, phenyl-F). Elemental Analysis: Theory (C: 32.53; N: 6.32; H: 2.12), Found (C: 32.63; N: 6.35; H: 2.07).

Re(O)Me(MesNHCH$_2$CH$_2$)$_2$NMe (1b). Triphenylphosphine (420.9 mg, 1.6 mmol), (MesNHCH$_2$CH$_2$)$_2$NMe (567.5 mg, 1.6 mmol), and methyltrioxorhenium (400 mg, 1.6 mmol) were added sequentially to a small reaction vial with about 2 mL of dichloromethane. The product was allowed to crystallize for 16 h to yield gray crystals (384 mg, 42.1%). ^{1}H NMR (CD_2Cl_2,

(44) Pestovsky, O.; Bakac, A. *J. Am. Chem. Soc.* **2003**, *125*(48), 14714–14715.
(45) Seymore, S. B.; Brown, S. N. *Inorg. Chem.* **2000**, *39*(2), 325–332.
(46) Hultzsch, K. C.; Hampel, F.; Wagner, T. *Organometallics* **2004**, *23* (11), 2601–2612.
(47) Kennedy-Smith, J. J.; Nolin, K. A.; Gunterman, H. P.; Toste, F. D. *J. Am. Chem. Soc.* **2003**, *125*(14), 4056–4057.

Table 2. Selected Crystallographic Data and Collection Parameters for Re(O)Me($C_6F_5NCH_2CH_2)_2$NMe (**1a**), Re(O)I($C_6F_5NCH_2CH_2)_2$NMe (**3a**), and Re(O)I-(MesNHCH$_2$CH$_2)_2$NMe (**3b**), and [(C_6F_5)(N(H)CH$_2$CH$_2)_2$NH(Me)][X], (X = ReO_4^-, or I^-), **4**

	complex **1a**	complex **3a**	complex **3b**	complex **4**
empirical formula	$C_{18}F_{10}H_{14}N_3ORe$	$C_{23}H_{33}IN_3ORe$	$C_{17}F_{10}H_{11}IN_3ORe$	$C_{17}H_{14}F_{10}I_{0.0784}N_3O_{3.6864}Re_{0.9216}$
formula wt	664.51	680.64	776.38	690.90
crystal system	orthorhombic	orthorhombic	triclinic	monoclinic
space group	*Pnma*	*Pnma*	$P\bar{1}$	*Cc*
a, Å	13.2914(4)	13.0515(5)	6.8210(3)	22.5189(5)
b, Å	22.0434(5)	21.5677(9)	8.1645(4)	7.4115(2)
c, Å	6.7339(2)	8.4982(3)	19.3225(10)	12.6984(3)
V (Å^3)	1972.95(9)	2392.17(16)	1020.13(9)	2028.73(9)
Z	4	4	4	4
D_{calcd}, g cm^{-3}	2.237	1.929	2.528	2.262
crystal size (mm)	0.25 × 0.23 × 0.06	0.30 × 0.12 × 0.08	0.12 × 0.08 × 0.06	0.17 × 0.05 × 0.02
*R*1, w*R*2 {$I > 2\sigma(I)$}	0.0298, 0.0538	0.0443, 0.1263	0.0269, 0.0595	0.0311, 0.0625
GOF	0.950	1.099	1.022	1.085

δ): 6.86 (s, 4H, Mes-*meta*-H), 4.37 (ddd, 2H, J = 4.4 Hz, 11.7 Hz, 23.4 Hz, NC*H*$_2$CH$_2$N), 3.56 (dd, 2H, J = 5.9 Hz, 12.8 Hz, NC*H*$_2$-CH$_2$N), 3.40 (s, 3H, N−C*H*$_3$), 3.10 (dd, 2H, J = 3.7 Hz, 11.0 Hz, NC*H*$_2$CH$_2$N), 2.69 (ddd, 2H, J = 6.2 Hz, 11.7 Hz, 22.7 Hz, NC*H*$_2$CH$_2$N), 2.39 (s, 3H, Re−C*H*$_3$), 2.28 (s, 6H, Mes-C*H*$_3$), 2.25 (s, 6H, Mes-C*H*$_3$), 1.84 (s, 6H, Mes-C*H*$_3$). ^{13}C NMR (CD_2Cl_2, δ): 136.39, 134.45, 133.89, 129.14, 71.98, 69.86, 49.36, 21.03, 18.90, 10.91. IR (KBr pellet) 958 cm^{-1} ($\nu_{Re\equiv O}$). Elemental Analysis: Theory(C: 50.68; N: 7.39; H: 6.38), Found-(C: 50.14; N: 7.35; H: 6.44). UV/vis (CH_2Cl_2 solution): λ_{max} (ε) = 327 (1064).

Re(O)Cl($C_6F_5NCH_2CH_2)_2$NMe (2a). 2,6-Lutidine (2.0 mL, 17.23 mmol), (C_6F_5NHCH$_2$CH$_2)_2$NMe (424.3 mg, 1.2 mmol), and Re(O)Cl$_3$(PPh$_3)_2$ (1.0 g, 1.2 mmol) were added to a 100 mL round-bottom flask with 60 mL of ethanol and stirred for 5 days. The resulting green solid was filtered and washed with excess diethyl ether to yield 638 mg product (77.6%). This complex was prepared by different route previously by Schrock and co-workers, (*Organometallics* **2000**, *19*, 2414−2614). ^{1}H NMR (CD_2Cl_2, δ) 4.18 (m, 2H, NC*H*$_2$CH$_2$N); 3.48 (m, 2H, NCH$_2$-C*H*$_2$N); 3.41 (s, 3H, N−C*H*$_3$); 3.27 (m, 4H, NC*H*$_2$C*H*$_2$N); UV/vis (CH_2Cl_2 solution): λ_{max} (ε) = 330 (866).

Re(O)Cl(MesNHCH$_2$CH$_2)_2$NMe (2b). 2,6-Lutidine (2.0 mL, 17.23 mmol), (MesNHCH$_2$CH$_2)_2$NMe (424.3 mg, 1.2 mmol), and Re(O)Cl$_3$(PPh$_3)_2$ (1.0 g, 1.2 mmol) were added to a 100 mL round-bottom flask with 60 mL of ethanol and refluxed for 16 h. The resulting yellow solid was filtered and washed with excess diethyl ether to yield 638 mg product (90.2%). ^{1}H NMR (CD_2Cl_2, δ) 6.87 (s, 2H, Mes-*meta*-H), 6.85 (s, 2H, Mes-*meta*-H), 3.95 (m, 2H, NC*H*$_2$CH$_2$N), 3.32 (s, 3H, N−C*H*$_3$), 3.19 (m, 6H, NC*H*$_2$C*H*$_2$N), 2.30 (s, 6H, Mes-C*H*$_3$), 2.25 (s, 6H, Mes-C*H*$_3$), 1.99 (s, 6H, Mes-C*H*$_3$). ^{13}C NMR (CD_2Cl_2, δ): 135.11, 134.77, 129.30, 129.08, 71.87, 66.619, 57.60, 19.50, 19.35. UV/vis (CH_2Cl_2 solution): λ_{max} (ε) = 340 (1460). m/z (ESI) 588.1923 ([M+H]$^+$. $C_{23}H_{34}ReN_3OCl$ requires 588.1915).

Re(O)I($C_6F_5NCH_2CH_2)_2$NMe (3a). Iododioxobis(triphenylphosphine)rhenium (314 mg, 0.35 mmol) and (C_6F_5NHCH$_2$-CH$_2)_2$NMe (251 mg, 0.558 mml) were added to a 10 mL round-bottom flask with 2 mL of CH_2Cl_2. The dark purple mixture was allowed to stir for a day at room temperature and a blue-greenish product was precipitated. This product was filtered to yield a blue-greenish solid, which was washed with 10 mL of hexanes to give 80 mg product (29%). ^{1}H NMR (acetone-d_6, δ) 4.22 (m, 2H, NC*H*$_2$CH$_2$N); 3.39 (m, 2H, NCH$_2$C*H*$_2$N); 3.30 (s, 3H, N−C*H*$_3$); 3.20 (m, 4H, NC*H*$_2$C*H*$_2$N); ^{19}F NMR (acetone-d_6, δ): −149.05 (m, 2F), −149.62 (m, 2F), −167.02 (m, 2F), −167.72 (m, 4F). UV/vis (CH_2Cl_2 solution): λ_{max} (ε) = 352 (3154). Elemental Analysis: Theory (C: 26.30; N: 5.41; H: 1.43), Found (C: 26.49; N:5.37; H: 1.50).

Re(O)I(MesNHCH$_2$CH$_2)_2$NMe (3b). Iododioxobis(triphenylphosphine)rhenium (521 mg, 0.554 mmol) and (MesNHCH$_2$-CH$_2)_2$NMe (196 mg, 0.554 mml) were added to a 100 mL round-bottom flask with 40 mL of benzene. The mixture was allowed to reflux for 12 h. After cooling to room temperature, the solution was filtered, and the solvent was removed under reduced pressure. The resulting solid was dissolved in methylene chloride, and hexanes was added to precipitate the product. The product was filtered and washed with ether to collect 150 mg of yellow-greenish solid (yield 40%). ^{1}H NMR (CD_2Cl_2, δ) 6.88 (s, 2H, Mes-*meta*-H); 6.85 (s, 2H, Mes-meta-H); 4.03 (m, 2H, NC*H*$_2$CH$_2$N); 3.25 (s, 3H, N−C*H*$_3$); 3.09 (m, overlap, 6H, NC*H*$_2$C*H*$_2$N); 2.34 (s, 6H, Mes-CH$_3$); 2.27 (s, 6H, Mes-CH$_3$); 1.97(s, 6H, Mes-CH$_3$). ^{13}C NMR (CD_2Cl_2, δ): 135.18, 134.98, 134.85, 129.03, 72.89, 66.08, 21.01, 20.11, 19.59. IR (KBr pellet) 933 cm^{-1} ($\nu_{Re\equiv O}$). m/z (ESI) 680.1264 ([M+H]$^+$. $C_{23}H_{34}Re-N_3OI$ requires 680.1271).

[(C_6F_5)N(H)CH$_2$CH$_2)_2$NH(Me)][X], (X = ReO_4^-, or I^-) 4. A 100 mL round-bottom flask was charged with Re(O)I-($C_6F_5NCH_2CH_2)_2$NMe (**3a**) (323 mg, 0.416 mmol), 4-cyano-pyridine-*N*-oxide (55 mg, 0.458 mmol), and CH_3CN (40 mL), and a homogeneous green solution was formed. The mixture was stirred at room temperature overnight, and color changes from green to yellow to brown and dark red were observed within 1 h. The solution was concentrated to 10 mL, and diethyl ether (30 mL) was added to form a red precipitate. A 220 mg red solid was collected through filtration and washed with diethyl ether (76% yield). ^{1}H NMR (CD_3CN, δ) 7.26 (br, 1H, N*H*-(Me)); 4.66 (m, 2H, (C_6F_5)N(*H*)); 3.66 (m, 4H, N(H)C*H*$_2$); 3.45 (m, 2H, (C_6F_5)N(H)CH$_2$C*H*$_2$); 3.33 (m, 2H, (C_6F_5)N(H)CH$_2$-C*H*$_2$); 2.97 (d, 3H, NH(C*H*$_3$); ^{19}F NMR (CD_3CN, δ): −160.14 (m, 4F), −166.85 (m, 4F), −173.22 (m, 2F).

Kinetics. Equal volumes of solutions of **2a** in acetonitrile (0.6 mM) and PyO (0.02−0.4 M) were mixed in a UV−vis cell at 298 K to give reaction solutions with half the loaded concentrations (30 μM in Re and 0.01−2 M in PyO. The decrease in absorbance of **2a** was monitored at 368 nm under these pseudo-first order conditions. The k_{obs} values were obtained by non-linear fitting of Abs$_{368}$ versus time to the equation: $Abs_t = Abs_\infty + (Abs_0 - Abs_\infty)\exp(-k_{obs}t)$. Plots of k_{obs} versus [PyO] showed saturation kinetics. Fits of the data to the appropriate rate law, eq 2, yielded a first order rate constant (k_5) and an apparent equilibrium constant (K'). Details for the rate law derivation are in the Supporting Information.

General Procedure for X-ray Determination. The sample was mounted on a nylon loop with a small amount of NVH immersion oil. The frame integration was performed using SAINT.[48] The resulting raw data was scaled and absorption corrected using a multiscan averaging of symmetry equivalent data using SADABS.[49]

The structure was solved by direct methods using the XS program (Table 2).[50] Most non-hydrogen atoms were obtained

(48) *SAINT*; Bruker-Nonius: Madison, WI, 2006.
(49) *SADABS*; Bruker-Nonius : Madison, WI, 2004.
(50) *SHELXTL, XS*; Bruker-AXS: Madison, WI, 2008.

from the initial solution. The remaining atom positions were recovered from a subsequent difference Fourier map. The hydrogen atoms were introduced at idealized positions and were allowed to ride on the parent atom. The structural model was fit to the data using full matrix least-squares based on F^2. The calculated structure factors included corrections for anomalous dispersion from the usual tabulation. The structure was refined using the XL program from SHELXTL,[51] graphic plots were produced using the NRCVAX crystallographic program suite. Additional information and other relevant literature references can be found in the reference section of the Facility's Web page (http://www.xray.ncsu.edu).

X-ray Structure Determination for Re(O)Me($C_6F_5NCH_2CH_2)_2$NMe (1a). All X-ray measurements were made on a Bruker-Nonius X8 Apex2 diffractometer at a temperature of 110 K. The unit cell dimensions were determined from a symmetry constrained fit of 9825 reflections with $5.96° < 2\theta < 64.28°$. The data collection strategy was a number of ω and φ scans which collected data up to 65.86° (2θ).

The final difference map showed a large peak ($5.31e^-/Å$) 2.07 Å from RE1 and 1.58 Å from C1. However, attempts to refine this peak as a bona fide atomic position (as either C or O) led to unreasonable displacement parameters.

X-ray Structure Determination for Re(O)I($C_6F_5NCH_2CH_2)_2$NMe (3a). All X-ray measurements were made on a Bruker-Nonius X8 Apex2 diffractometer at a temperature of 110 K. The unit cell dimensions were determined from a symmetry constrained fit of 9922 reflections with $5.26° < 2\theta < 63.62°$. The data collection strategy was a number of ω and φ scans which collected data up to 64.74° (2θ).

X-ray Structure Determination for Re(O)I($MesNCH_2CH_2)_2$NMe (3b). All X-ray measurements were made on a Bruker-Nonius X8 Apex2 diffractometer at a temperature of 173 K. The unit cell dimensions were determined from a symmetry constrained fit of 9881 reflections with $5.16° < 2\theta < 59.7°$. The data collection strategy was a number of ω and φ scans which collected data up to 66.22° (2θ).

The molecule resides on a crystallographic mirror which imposed a positional disorder in *N*-methyl group (atom C12) which further induced a positional disorder between atoms C11 and C11′.

X-ray Structure Determination for [(C_6F_5)(N(H)$CH_2CH_2)_2$NH(Me)][X], (X = ReO_4^-, or I^-), 4. All X-ray measurements were made on a Bruker-Nonius Kappa Axis X8 Apex2 diffractometer at a temperature of 110 K. The unit cell dimensions were determined from a symmetry constrained fit of 9980 reflections with $5.82° < 2\theta < 64.32°$. The data collection strategy was a number of ω and φ scans which collected data up to 70.54° (2θ).

The structure exhibits a compositional disorder between ReO_4^- and I^-. The occupancies of the perrhenate anion and the iodide anion were refined and normalized to an occupancy of 1.0. The occupancy of the perrhenate was refined to be 0.9216(14). The rhenium atom position and the iodine atom position were offset by 1.12 Å.

Acknowledgment. Acknowledgement is made to North Carolina State University, ACS-PRF Type-G (PRF# 47820-G3), and the ORAU Ralph E. Powe Junior Faculty Enhancement Award for financial support. The authors thank the Department of Chemistry of North Carolina State University and the State of North Carolina for funding the purchase of the Apex2 diffractometer.

Supporting Information Available: X-ray data for **3b** and CIF files for **1a**, **3a**, **3b**, and **4**. Rate law derivation for Scheme 3C and selected UV−vis spectra. This material is available free of charge via the Internet at http://pubs.acs.org.

(51) *SHELXTL, XL*; Bruker-AXS: Madison, WI, 2008.